

Elasto-Plastic MLPG Method for Micromechanical Modeling of Heterogeneous Materials

Isa Ahmadi¹, M.M. Aghdam²

Abstract: In this study, a truly meshless method based on the meshless local Petrov-Galerkin method is formulated for analysis of the elastic-plastic behavior of heterogeneous solid materials. The incremental theory of plasticity is employed for modeling the nonlinearity of the material behavior due to plastic strains. The well-known Prandtl-Reuss flow rule of plasticity is used as the constitutive equation of the material. In the presented method, the computational cost is reduced due to elimination of the domain integration from the formulation. As a practical example, the presented elastic-plastic meshless formulation is employed for micromechanical analysis of the unidirectional composite material. A quarter of the fiber surrounded in the matrix in a square array is considered as the Representative Volume Element (RVE). The fully bonded fiber-matrix interface condition is assumed and the continuity of displacement and reciprocity of traction are imposed to the interface. A predictor-corrector numerical integration method is used for the solution of the discretized equations of the problem. The numerical results show excellent agreement with the predictions of the finite element analysis.

Keywords: Meshless method; Elasto-Plastic behavior; Heterogeneous material; Incremental theory of plasticity; Micromechanics of composites.

1 Introduction

Recently, meshless methods become very attractive for the solution of the boundary value problems. The advantages of meshless methods such as the absence of mesh of elements, higher degree of continuity in the solution field, and capability to handle moving boundary make meshless methods efficient and promising methods comparing other discretization methods. In the meshless methods, no predefined

¹ Corresponding author, Advanced Materials and Computational Mechanics Lab., Department of Mechanical Engineering, University of Zanjan, 45371-38791, Zanjan, Iran, E-mail: i_ahmadi@znu.ac.ir, Tell: +98 24 3305 4058

² Department of Mechanical Engineering, Amirkabir University of Technology, Tehran, Iran

mesh of elements are needed among the nodes for the construction of the trial or test functions and nodes can be added and removed without remeshing of elements. Therefore, one of the main objectives of the meshless methods is to eliminate or alleviate various difficulties related to the elements such as meshing and remeshing of domain and locking and distortion of elements in large deformation problems. Another advantage of meshless approximations with respect to conventional discretization methods such as finite element method is related to the continuity of approximated fields. In the meshless methods, C^1 continuity of trial (shape) functions can be obtained very easily with respect to the other discretization methods such as in the finite element method.

In the last two decades, various versions of meshless methods have been developed. Among them one can refer to the diffuse element method [Nayroles, Touzot, and Villon (1992)], element free Galerkin (EFG) method [Belytschko, Lu, and Gu (1994)], reproducing kernel particle method [Liu, Chen, Chang, and Belytschko (1996)], HP-meshless cloud method [Duarte and Oden (1996)], boundary node method (BNM) [Mukherjee and Mukherjee (1997)], natural element method [Sukumar, Moran, and Belytschko (1998)] local boundary integral equation (LBIE) method [Zhu, Zhang, and Atluri (1998)], meshless local Petrov-Galerkin (MLPG) method [Atluri and Zhu (1998)] and local point interpolation method (LPIM) [Gu and Liu (2002)]. Recently, Dong, Alotaibi, Mohiuddine, and Atluri (2014) studied variety of computational methods, such as Collocation method, Finite Volume method, Finite Element method, Boundary Element Method and MLPG method and present them in a unified way.

The main applications of the meshless methods in the literature include solution of linear elasto-static/dynamic problems [Atluri and Zhu (2000); Long, Liu, and Hu (2006); Sladek, Sladek, and Solec (2009)], plate bending [Gu and Liu (2001); Belinha and Dinis (2006)], fracture mechanics [Belytschko, Lu, and Gu (1995); Ching and Batra (2001)], metal forming [Li and Belytschko (2001)], heat transfer [Singh, Sandeep, and Prakash (2002); Sladek, Sladek, and Atluri (2004); Sladek, Sladek, Tan, and Atluri (2008), Ahmadi and Aghdam (2011a)] and fluid flow problems [Lin and Atluri (2001)] and micromechanics of composite materials [Ahmadi and Aghdam (2010)]. Recently, Sladek, Stanak, Han, Sladek and Atluri, (2013) presented an excellent review on the MLPG methods and its application in the solution of various problems in the field of Engineering and science.

Some researchers have developed meshless methods for the analysis of the elastic-plastic behavior of materials. These methods include application of the radial point interpolation method (RPIM) [Dai, Liu, Han, and Li (2006); Gu, Wang, Lam, and Dai (2007)] and meshless finite point method (FPM) [Perez Pozo, Perazzo, and Angulo (2009)] based on the deformational theory for inelastic analysis of materi-

als. In all of these methods, the Hencky's total deformation theory is used to define the effective material parameters such as effective Young's modulus and Poisson's ratio of the material in the plastic region and therefore these methods are in fact pseudo-elastic methods for elastic-plastic analysis of the continuum materials.

Han, Rajendran, and Atluri (2005) present a MLPG approach for solution of non-linear problems including large deformations and rotations. Then Batra and Porfiri (2008) studied the behavior of a rubber like materials and Heaney, Augarde, and Deeks (2010) extended a hybrid MLPG formulation for analysis of elasto-plastic behavior of materials, but few details of the formulation and implementation of the plastic behavior is seen in these papers. However development of the MLPG method, and EFG method, for problems with material nonlinearity (e.g. elasto-plasticity) has to date been limited.

On the other hand, the elastic-plastic behavior of heterogeneous materials is studied by analytical and numerical methods. Generally macro-mechanical and micro-mechanical approaches are used to model the elastic-plastic behavior of the fibrous composite materials as an example of the heterogeneous material. In the macro-mechanical approaches the heterogeneous nature of the composite material is replaced by a homogenous medium and in the micro-mechanical approaches, the composite is treated as a heterogeneous material with different phases. In the micro-mechanical approaches, both analytical [Hill (1964); Hill (1965); Hung (1973); Coker, Ashbaugh, and Nicholas (1993); Dvorak and Bahei-El-Din (1979); Dvorak and Bahei-El-Din (1982); Aboudi (1996); Robertson and Mall (1993); Arnoled, Pindera, and Wilt (1996); Sun and Chen (1991)] and numerical finite element methods [Adams (1970); Foye (1973); Lin, Salinas, and Ito (1972); Aghdam, Smith, and Pavier (2000); Zhu and Sun (2003); Ding, Tong, and Shen (2005); Taliercio (2005)] are developed for analysis of the elastic-plastic behavior of composite materials. Analytical methods usually involve more simplifications and are not able to predict the micro-stresses and micro-strains in the composite. Numerical methods usually involve fewer simplifications and are able to predict the micro-stress/strain distribution in the composite materials. The numerical methods used for the micro-mechanical analysis of elastic-plastic behavior of composite materials mainly include the finite element method.

In this study a meshless method formulation based on the MLPG5 [Atluri and Shen (2002)] is presented for analysis the elasto-plastic behavior of solid materials. The method is suitable for macro-mechanical and micromechanical analysis of elastic-plastic behavior of the heterogeneous materials. The incremental theory of plasticity is employed for modelling the elastic plastic loading and the Prandtl-Reuss flow rule of plasticity is applied for formulation of the plastic behavior of the material. In the present method the domain integration over the local sub-domains is totally

eliminated and the computational efforts are substantially decreased. The presented elastic-plastic meshless method is employed for the analysis of micro-stresses and micro-strains in the unidirectional Boron-Aluminium (B/Al) metal matrix composite. The convergence study of the method and comparison of the computational efforts show that the presented method is an efficient and less costly method. Also comparison of the numerical results of this study with the finite element method show excellent agreement with the predictions of the finite element method.

2 Meshless formulation

In a continuum body with domain Ω which is in the static equilibrium condition, all of the sub-particles named Ω_s^I that are located inside the body are in the equilibrium condition. In the absence of body force, the equilibrium equations for a sub-particle (sub-domain) Ω_s^I located inside the global domain Ω and subjected to traction on its surface could be written as [Atluri (2004); Sladek, Sladek, and Solek (2009); Ahmadi and Aghdam (2011b)]

$$\int_{\partial\Omega_s^I} t_i d\Gamma = 0, \quad i = 1, 2, 3 \quad (1)$$

where $\partial\Omega_s^I$ is the boundary of the local sub-domain i.e. Ω_s^I and t_i is the traction vector on the boundary of the local sub-domain. The boundary of the sub-domain i.e. $\partial\Omega_s^I$ could have arbitrary shape and circular sub-domain is used in this study. Using the Cauchy formula the traction t_i on the boundary of the sub-domain can be obtained as

$$t_i = \sigma_{ij} n_j \quad (2)$$

in which $\mathbf{n} = (n_1, n_2, n_3)$ is the outward unit normal vector on the boundary of the local sub-domain. The equilibrium equation in (1) could be written as

$$\int_{L_s^I} t_i d\Gamma + \int_{\Gamma_{su}^I} t_i d\Gamma = - \int_{\Gamma_{st}^I} \bar{t}_i d\Gamma \quad (3)$$

in which L_s^I is the part of the local boundary ($\partial\Omega_s^I$) which is located completely inside the global domain, Γ_{st}^I and Γ_{su}^I are the parts of local boundary that coincide with the global traction boundary and with the global essential boundary, respectively. In Eq. (3), \bar{t}_i is the prescribed traction on the traction (natural) boundary of the sub-domain, i.e. Γ_{st}^I . It is seen that there is no domain integration in the formulation in Eq. (3). By avoiding the domain integration, the computational efforts of the method are reduced substantially.

3 Elastic-plastic constitutive equations

The incremental form of stress-strain constitutive equations in the elastic-plastic zone can be written as

$$d\sigma_{ij} = 2G(d\epsilon_{ij} + \frac{\nu}{1-2\nu}d\epsilon_{kk}\delta_{ij} - d\epsilon_{ij}^p) \quad (4)$$

in which $d\epsilon_{ij}$ denotes the incremental total strain, $d\epsilon_{ij}^p$ is the plastic part of the incremental strain, G and ν denote the shear modulus and Poisson ratio of the material, respectively. The Prandtl-Reuss flow theory of plasticity [Mendelson (1970)] is applied in this study. According to the Prandtl-Reuss flow rule of plasticity, the plastic strain increment $d\epsilon_{ij}^p$ in any time of loading is proportional to the instantaneous stress deviation S_{ij} as

$$d\epsilon_{ij}^p = S_{ij}d\lambda \quad (5)$$

where $d\lambda$ is a nonnegative constant which may vary throughout the loading history and S_{ij} is the stress deviator tensor which is defined as

$$S_{ij} = \sigma_{ij} - \frac{1}{3}\sigma_{kk}\delta_{ij} \quad (6)$$

The desired stress-strain relation in Eq. (4) will be known if $d\lambda$ is known. In the appendix, it is shown in detail that $d\lambda$ can be obtained as

$$d\lambda = \frac{S_{ij}d\epsilon_{ij}}{\frac{2}{3}\sigma_e^2(1 + \frac{1}{3G}M_T)} \quad (7)$$

in which σ_e is the effective stress and

$$M_T = d\sigma_e/d\epsilon_p = \left(\frac{1}{E_T} - \frac{1}{E}\right)^{-1} \quad (8)$$

where $E_T = d\sigma/d\epsilon$ is the hardening modulus of the material in the plastic region. The effective stress σ_e and the effective plastic strain increment $d\epsilon_p$ are defined in Eq. (A2) in the appendix.

By substitution of $d\lambda$ from Eq. (7) into Eq. (5) and the subsequent result into Eq. (4), the incremental stress-strain relation can be obtained as

$$d\sigma_{ij} = 2G(d\epsilon_{ij} + \frac{\nu}{1-2\nu}d\epsilon_{kk}\delta_{ij} - \frac{S_{kl}S_{ij}}{\frac{2}{3}\sigma_e^2(1 + \frac{1}{3G}M_T)}d\epsilon_{kl}) \quad (9)$$

in which $E = 2G(1 + \nu)$ is the Young's modulus of the material and P is defined as

$$P = \frac{2}{3}\sigma_e^2\left(1 + \frac{1}{3G}M_T\right) \quad (16)$$

Eq. (10) shows the general form of the stress-strain relation in the elastic and plastic region. It is seen that in the elastic region \mathbf{D} is reduced to \mathbf{D}^e and in plastic region $\mathbf{D} = \mathbf{D}^e + \mathbf{D}^p$. It is clear that \mathbf{D}^p varies point by point because it depends on the state of stress of the point and also it is not constant during the loading history.

4 Kinematic assumption

In this study the unidirectional composite material reinforced by long and parallel fibers which is subjected to normal loading conditions in the transverse and axial direction is considered. The appropriate kinematic assumption for the micromechanical analysis of composites reinforced by long and parallel fibers is the state of generalized plane strain (GPS) condition [Adams and Crane (1984)]. In the generalized plane strain condition, displacements occur in all three directions and the normal strain in the fiber (x_3) direction, i.e. normal to the plane is constant. Assuming the generalized plane strain condition, the displacement field within the RVE can be considered as

$$\begin{aligned} u_1 &= u_1(x_1, x_2) \\ u_2 &= u_2(x_1, x_2) \\ u_3 &= u_{3ref}(x_1, x_2) + \varepsilon_0 x_3 \end{aligned} \quad (17)$$

where u_1, u_2 and u_3 are displacements in the x_1, x_2 and x_3 directions, respectively and ε_0 is an unknown constant strain in the fiber (x_3) direction and u_{3ref} handle the axial deformation due to axial shear γ_{13} and γ_{23} . In this study, the axial shear is not considered in the analysis and only the transverse and axial normal loading is considered. In this case u_{3ref} is eliminated from the deformation field of the RVE and so u_{3ref} is not considered in the analysis. The strain component in the RVE can be obtained based on the infinitesimal linear theory of elasticity and the displacement field in Eq. (17). It must be mentioned that by elimination u_{3ref} , the out of plane shear strains i.e. ε_{13} and ε_{23} vanish and so it is concluded that the shear stresses in the fiber direction will be vanished, i.e. $\sigma_{13} = \sigma_{23} = 0$.

4.1 Boundary and interface conditions

In general the periodic boundary conditions must be considered for the RVE. In this study the axial and transverse normal loading is considered. For transverse and axial normal loading, the periodic boundary conditions for the RVE change to

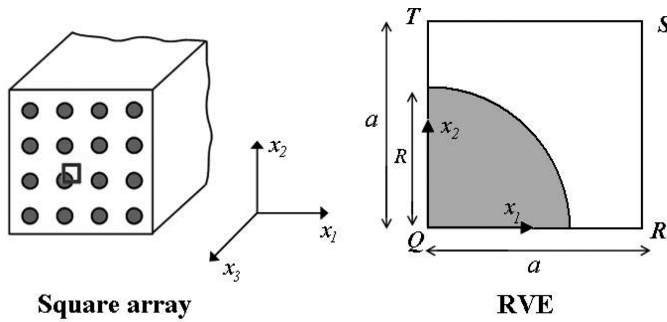


Figure 1: The cross section of the composite with square array, fiber distribution and corresponding RVE.

symmetric boundary conditions. In the transverse and axial normal loading of the composite, a typical RVE as shown in Fig. 1 deforms in such a way that after deformation plane sections in the edges of the RVE remain plane. So, due to periodicity and symmetry of the model, the corresponding boundary conditions on the edges of the RVE for transverse and axial normal loading can be considered as

$$\begin{aligned}
 u_1(x_1 = 0) &= 0, \\
 u_1(x_1 = a) &= \bar{u}_1, \\
 u_2(x_2 = 0) &= 0, \\
 u_2(x_2 = a) &= \bar{u}_2,
 \end{aligned} \tag{18}$$

where \bar{u}_i is constant displacement in the x_i direction on the boundary and is unknown during the solution. In this study, the fiber-matrix interface in the RVE is assumed to be fully bonded. For the fully bonded fiber-matrix interface, the displacement continuity and the traction reciprocity must be imposed to the fiber-matrix interface as

$$\begin{aligned}
 \mathbf{u}^f &= \mathbf{u}^m \\
 \mathbf{t}^f + \mathbf{t}^m &= 0
 \end{aligned} \tag{19}$$

where \mathbf{u} is the displacement vector and \mathbf{t} is the traction vector on the interface and superscript f and m denote the fiber and matrix, respectively.

4.2 Loading conditions

In this study, it is assumed that the external stresses which are applied to the RVE are known and the displacement and stresses on the right and top edge of the RVE is unknown. It is supposed that the average external normal stress (macro stress)

which is applied to the composite in the x_i direction is $\bar{\sigma}_i$. So, the average stress on the right side, top side and over the area of the RVE is equal to the applied external stress as

$$\begin{aligned} \frac{1}{a} \int_{x_2=0}^{x_2=a} \sigma_1 dx_2 &= \bar{\sigma}_1 && \text{On the right side at } x_1 = a \\ \frac{1}{a} \int_{x_1=0}^{x_1=a} \sigma_2 dx_1 &= \bar{\sigma}_2, && \text{On the top side at } x_2 = a \\ \frac{1}{a^2} \iint_{RVE} \sigma_3 dx_1 dx_2 &= \bar{\sigma}_3 && \text{Over the RVE :} \end{aligned} \quad (20)$$

These equations represent the external loading conditions which apply to the sides of the RVE and should be considered in the solution of the RVE.

5 Solution

5.1 Moving least square (MLS) approximation

One of the well-known methods used for approximation of the field variable $u(\mathbf{x})$ over a number of randomly located nodes within the domain is the moving least squares (MLS) technique which is described in Atluri and Zhu (1998). In the MLS approximation, the nodal interpolation form of field variable $u(\mathbf{x})$ may be expressed as

$$u^h(\mathbf{x}) = \sum_{I=1}^N \phi^I(\mathbf{x}) \hat{u}^I \quad (21)$$

where $\phi^I(\mathbf{x})$ is usually called the shape function of the MLS approximation corresponding to node I and \hat{u}^I is the fictitious nodal value of the field variable in node I . It should be noted that the shape functions derived from the MLS approximation do not satisfy the Kronecker delta function criterion, i.e. $\phi^I(\mathbf{x}_J) \neq \delta_{IJ}$ and $u^h(\mathbf{x}_I) \neq \hat{u}^I$.

5.2 Numerical discretization

In the case of the generalized plane strain condition in which the normal strain in the x_3 direction i.e. $\epsilon_{33} = \epsilon_0$ is constant and $\epsilon_{13} = \epsilon_{23} = 0$, the stress-strain form of the constitutive equations for fiber and matrix can be written using Eq. (10) to (15) as

$$\begin{aligned} d\boldsymbol{\sigma} &= \mathbf{D}d\boldsymbol{\epsilon} + \hat{\mathbf{D}}d\epsilon_0 \\ \sigma_{33} &= \hat{\mathbf{D}}^T d\boldsymbol{\epsilon} + C\epsilon_0 \end{aligned} \quad (22)$$

in which $d\boldsymbol{\sigma}$ and $d\boldsymbol{\epsilon}$ are defined as

$$\begin{aligned} d\boldsymbol{\sigma} &= \{d\sigma_{11} \quad d\sigma_{22} \quad d\sigma_{12}\}^T \\ d\boldsymbol{\epsilon} &= \{d\epsilon_{11} \quad d\epsilon_{22} \quad 2d\epsilon_{12}\}^T, \end{aligned} \quad (23)$$

and \mathbf{D} , $\hat{\mathbf{D}}$ and C are defined as

$$\mathbf{D} = \mathbf{D}^e + \beta \mathbf{D}^p, \quad \hat{\mathbf{D}} = \hat{\mathbf{D}}^e + \beta \hat{\mathbf{D}}^p, \quad C = C^e + \beta C^p \quad (24)$$

in which

$$\mathbf{D}^e = \frac{E}{(1+\nu)(1-2\nu)} \begin{bmatrix} 1-\nu & & \text{Sym.} \\ \nu & 1-\nu & \\ 0 & 0 & \frac{(1-2\nu)}{2} \end{bmatrix}, \quad (25)$$

$$\mathbf{D}^p = -\frac{E}{(1+\nu)P} \begin{bmatrix} S_{11}^2 & & \text{Sym.} \\ S_{11}S_{22} & S_{22}^2 & \\ S_{11}\sigma_{12} & S_{22}\sigma_{12} & \sigma_{12}^2 \end{bmatrix}$$

$$\hat{\mathbf{D}}^e = \frac{E}{1+\nu} \left\{ \frac{\nu}{1-2\nu} \quad \frac{\nu}{1-2\nu} \quad 0 \right\}^T \quad (26)$$

$$\hat{\mathbf{D}}^p = -\frac{E}{(1+\nu)P} \{S_{11}S_{33} \quad S_{22}S_{33} \quad S_{33}\sigma_{12}\}^T$$

$$C^e = \frac{E}{1+\nu} \left(\frac{1-\nu}{1-2\nu} \right), \quad C^p = -\frac{E}{1+\nu} \frac{S_{33}^2}{P} \quad (27)$$

In the generalized plane strain condition, the increment of the traction, i.e. $d\mathbf{t}$ on the boundary of the sub-domain in the matrix form can be obtained using Eq. (2) and Eq. (22) as

$$d\mathbf{t} = \mathbf{N}d\boldsymbol{\sigma} = \mathbf{N}\mathbf{D}d\boldsymbol{\varepsilon} + \mathbf{N}\hat{\mathbf{D}}d\varepsilon_0 \quad (28)$$

Substituting traction from Eq. (28) into Eq. (3) and using the MLS approximation lead to the discretized form of the governing equations as

$$-\sum_{J=1}^N \int_{L_s^J} \mathbf{N}\mathbf{D}\mathbf{B}^J d\hat{\mathbf{u}}^J d\Gamma - \sum_{J=1}^N \int_{\Gamma_{su}^J} \mathbf{N}\mathbf{D}\mathbf{B}^J d\hat{\mathbf{u}}^J d\Gamma = \int_{\Gamma_{st}^J} \bar{\mathbf{t}} d\Gamma + d\varepsilon_0 \left(\int_{L_s^J} \mathbf{N}\hat{\mathbf{D}} d\Gamma + \int_{\Gamma_{su}^J} \mathbf{N}\hat{\mathbf{D}} d\Gamma \right) \quad (29)$$

where

$$\mathbf{B}^J = \begin{bmatrix} \phi_{,1}^J & 0 & \phi_{,2}^J \\ 0 & \phi_{,2}^J & \phi_{,1}^J \end{bmatrix}^T, \quad \mathbf{N} = \begin{bmatrix} n_1 & 0 & n_2 \\ 0 & n_2 & n_1 \end{bmatrix} \quad (30)$$

in which $\mathbf{n} = (n_1, n_2, 0)$ is the outward unit normal on the boundary of the local sub-domain and $\phi_{,i}^J$ denotes the partial derivative of $\phi^J(\mathbf{x})$ with respect to x_i . Eq. (29) can be written in the standard form of linear algebraic equations as

$$\sum_{J=1}^N \mathbf{K}_{IJ} d\hat{\mathbf{u}}^J = d\mathbf{f}_I \quad (31)$$

It is seen that the domain integration is totally eliminated in this formulation.

It should be mentioned here that Gauss quadrature method is used to evaluate the integrations in Eq. (29) to get the stiffness matrix \mathbf{K} and force vector \mathbf{f} in Eq. (31). Eq. (29) involves integration on the boundary of the sub-domains. Circular sub-domain around the nodes is used in this study. The integration on the arc of the circles is carried out based on the Gauss point. For each Gauss quadrature point \mathbf{x}_Q which is located on the boundary of the sub-domain, the meshless shape functions are constructed to obtain the integrand. It means that \mathbf{K} and \mathbf{f} are obtained based on all quadrature points. Hence, for the Gauss quadrature point \mathbf{x}_Q that is in the elastic region of the material $\beta = 0$ and so $\mathbf{D} = \mathbf{D}^e$ and for the Gauss point that is in the plastic region $\beta = 1$ and so $\mathbf{D}(\mathbf{x}_Q) = \mathbf{D}^e + \mathbf{D}^p(\mathbf{x}_Q)$. Hence, $\mathbf{D}(\mathbf{x}_Q)$, $\hat{\mathbf{D}}(\mathbf{x}_Q)$ and $C(\mathbf{x}_Q)$ should be the material parameter matrix at the Gaussian quadrature point.

5.3 Treatment of material discontinuity and boundary conditions

In the meshless methods there is no mesh of elements and the material interface cannot be defined based on the elements. In this paper, the selected RVE is considered as two homogeneous bodies. In order to treat the material discontinuity at the fiber-matrix interface, two sets of nodes are assigned to the fiber-matrix interface at the same location with different material properties. One set which is dedicated to the fiber known as I^f while the other set is related to the matrix denoted by I^m . By this, the interface conditions in Eq. (20) for all of the nodes that are located at the interface in the same location can be written in the discretized form as

$$\sum_{J=1}^{N_f} (\Phi^J(x_{I^f})d\hat{u}^J)^f - \sum_{J=1}^{N_m} (\Phi^J(x_{I^m})d\hat{u}^J)^m = 0 \quad (32)$$

$$\sum_{J=1}^{N_f} \mathbf{N}(\mathbf{D}\mathbf{B}^J(x_{I^f})d\hat{u}^J + \hat{\mathbf{D}}d\boldsymbol{\epsilon}_0)^f + \sum_{J=1}^{N_m} \mathbf{N}(\mathbf{D}\mathbf{B}^J(x_{I^m})d\hat{u}^J + \hat{\mathbf{D}}d\boldsymbol{\epsilon}_0)^m = 0 \quad (33)$$

where N_f is the total number of nodes in the fiber and N_m is the total number of nodes in the matrix. Also according to Eq. (18) the essential boundary conditions on the bottom and left side of the RVE can be imposed in discrete form as

$$\sum_{J=1}^N \phi^J(x_I)d\hat{u}_i^J = 0 \quad (34)$$

and the displacement conditions on the top and right sides of the RVE may be imposed as

$$\sum_{J=1}^N \phi^J(x_I)d\hat{u}_i^J - d\bar{u}_i = 0 \quad (35)$$

where $d\bar{u}_i$, $i = 1, 2$ is the increment of the constrained displacement on the right and top side of the RVE, respectively. Equations (32) to (35) can be directly imposed to the global stiffness and the force matrix of the problem. For instance, in order to

impose Eq. (34) to the node I that is located on the bottom edge and the left edge, the row of the global stiffness and force matrix in Eq. (31) which is related to the node I should be changed to

$$\begin{aligned} \mathbf{K}_{IJ} &= \phi^J(\mathbf{x}_I) \\ f_I &= 0 \end{aligned} \quad (36)$$

Furthermore, similar replacement in the global stiffness and the force matrix should be applied to all interface nodes based on the interface conditions in Eq. (32) and Eq. (33) and for all the constrained nodes based on Eq. (34) and Eq. (35). This leads to direct enforcement of the boundary and interface conditions to the system of equations. Finally, it is worth mentioning that the final stiffness matrix in this method is banded and asymmetric.

5.4 Implementation of the method (solution procedure)

In order to obtain the distribution of stress and displacement in the RVE, the differential equations of the problem must be integrated. In this study, a predictor-corrector method for numerical integration is used for solving the differential equations of the problem. The idea behind the predictor-corrector methods is using a suitable combination of an explicit and an implicit technique to obtain a method with better convergence characteristics. The procedure for solving the governing equations of the problem can be explained as below. For instance, suppose that an external load F is applied to the structure.

1- In the first step, a full elastic analysis is done and the load that causes the initial yield of the structure is predicted. This load is named F_Y . When F_Y is greater than the applied load F , i.e. $F_Y > F$, the structure is in the elastic region and the solution is finished. If F is greater than F_Y , i.e. $F > F_Y$, then the following procedure should be carried out.

2- The loading path is divided into a number of load increments $\Delta F_i (i = 1, 2, \dots, N)$ and the first load increment ΔF_1 is taken equal to F_Y , i.e. $\Delta F_1 = F_Y$. For the first load step an elastic analysis is done for obtaining displacements, stresses and effective stress, σ_e , at the end of the first load step ΔF_1 .

3- For the i^{th} load increment ($i > 1$), the plastic strain will be observed in some local domains inside the global domain, thus the elastic-plastic differential equations of the problem in Eq. (29) should be solved. As said before, for the gauss points that located in plastic regions the plastic index $\beta = 1$ and therefore $\mathbf{D} = \mathbf{D}^e + \mathbf{D}^p$. As mentioned before, a predictor-corrector method is employed for solving of the governing equations of the system. In the predictor-corrector method the results at the end of the i^{th} load step are obtained from the results of $(i - 1)^{\text{th}}$ load step in two stages.

5.4.1 Prediction stage

In the *Prediction stage* the results at the end of the i^{th} load step are predicted from the results of the $(i - 1)^{\text{th}}$ step as follow

$$\boldsymbol{\sigma}_0 = \boldsymbol{\sigma}_{(i-1)} \quad (37)$$

$$d\hat{\mathbf{u}}^{(p)} = (\mathbf{K}(\boldsymbol{\sigma}_0))^{-1} d\mathbf{f}_{(i)} \quad (38)$$

$$d\boldsymbol{\sigma}^{(p)} = \mathbf{D}(\boldsymbol{\sigma}_0)d\boldsymbol{\varepsilon}^{(p)} + \hat{\mathbf{D}}(\boldsymbol{\sigma}_0)d\boldsymbol{\varepsilon}_0^{(p)} \quad (39)$$

$$\boldsymbol{\sigma}^{(p)} = \boldsymbol{\sigma}_{(i-1)} + d\boldsymbol{\sigma}^{(p)} \quad (40)$$

in which the superscript (p) denotes the predicted values.

5.4.2 Correction stage

In this stage, the results at the end of the i^{th} load step are corrected using the results of the $(i - 1)^{\text{th}}$ step and the previous predicted values of the i^{th} load step i.e. $\boldsymbol{\sigma}^{(p)}$ which is obtained in Eq. (40) as follow

$$d\hat{\mathbf{u}}^{(c)} = 0.5[\mathbf{K}(\boldsymbol{\sigma}_0) + \mathbf{K}(\boldsymbol{\sigma}^{(p)})]^{-1} d\mathbf{f}_{(i)} \quad (41)$$

$$d\boldsymbol{\sigma}^{(c)} = 0.5(\mathbf{D}(\boldsymbol{\sigma}_0) + \mathbf{D}(\boldsymbol{\sigma}^{(p)}))d\boldsymbol{\varepsilon}^{(c)} + 0.5(\hat{\mathbf{D}}(\boldsymbol{\sigma}_0) + \hat{\mathbf{D}}(\boldsymbol{\sigma}^{(p)}))d\boldsymbol{\varepsilon}_0^{(c)} \quad (42)$$

in which the superscript (c) denotes the corrected values.

4- The total displacement and the total stress at the end of the i^{th} load step can now be obtained as

$$\mathbf{u}_{(i)} = \mathbf{u}_{(i-1)} + d\mathbf{u}^{(c)} \quad (43)$$

$$\boldsymbol{\sigma}_{(i)} = \boldsymbol{\sigma}_{(i-1)} + d\boldsymbol{\sigma}^{(c)} \quad (44)$$

5- Steps 3 to 4 should be repeated until the applied load $F_i = F_{i-1} + \Delta F_i$ reaches the final level of the applied load F . The updated overall stress at each load level can be plotted against the overall strain in the same load level in order to obtain the stress-strain curve of the composite during the specified loading interval.

6 Numerical results and dissections

Among the metal matrix composites, those based on the Aluminium and Titanium alloys are seem promising composites for obtaining a light material with enhanced mechanical properties. In this study, the unidirectional Boron/Aluminum (B/Al) metal matrix composite with 45.5% Fiber volume fraction (FVF) is considered. It is assumed that the Boron fibers have circular cross-section and are packed in

the square array arrangement. The 45.5% FVF is chosen in such a way that the comparison with the open literature is possible. The fibers are assumed to be elastic up to the fracture point. The rate independent behavior is assumed for the materials. The Aluminum matrix in the composite system is assumed to have the elastic with linear work hardening behavior. The strain hardening module after yielding of the matrix is taken as $E_T^m = 1.17$ GPa and the stress in which the first yield is seen in the aluminum matrix (yield stress) is assumed to be $\sigma_Y^m = 142$ MPa [Huang (2000)]. The mechanical properties of the fiber and matrix are tabulated in Table 1.

Table 1: The elastic properties of Boron fiber and Aluminum matrix in Boron/Aluminum composite system [Adams and Crane (1984)].

Material Property	E (Gpa)	E_T (Gpa)	ν	σ_Y (MPa)	Volume Fraction
Boron (B)	397	397	0.21	–	0.455
Aluminum (Al)	71	1.17	0.32	142	0.545

6.1 Convergence study and CPU time

The rate of convergence and the CPU time of the presented method are studied in this section. Fig. 2 shows the transverse displacement (u_1) on the right hand side ($x_1 = a$) of the RVE for transverse loading as $\sigma_1 = 180$ MPa for various numbers of nodes in the RVE. It must be noticed that the u_1 displacement is the same for all the nodes on the right side of the RVE. To comparison, another analysis was

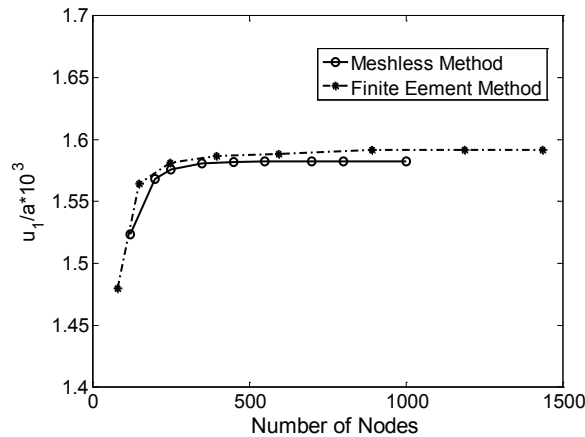


Figure 2: Convergence study of the meshless and finite element method with respect to number of nodes, ($\sigma_1^* = 180$ MPa).

also carried out using the commercial finite element code ANSYS by 4 node plane elements. Details of the modeling and imposing boundary conditions can be found in Aghdam, Smith, and Pavier (2000). The prediction of the analysis with ANSYS is also included in Fig. 2. It is seen that very good convergence can be achieved by using about 500 nodes in the meshless method while FE analysis requires more than 1000 nodes for the same level of convergence. Therefore, in all presented results in this section 500 or some more nodes are used for meshless and 1180 nodes (1092 elements) are used for FE analyses, respectively.

Moreover, the efficiency of the presented method is examined with respect to the MLPG method which first was introduced by Atluri and Zhu (2000). This MLPG method [Atluri and Zhu (2000)] uses symmetric weak formulation and domain integration in the local sub-domains and is so-called MLPG1 method [Atluri and Shen (2002)]. In order to examine the efficiency of the presented method with respect to the MLPG1, a same code is developed for analysis of the problem based on the conventional MLPG formulation. The node distribution, MLS approximation and size of sub-domains are chosen exactly the same in both codes. Table 2 compares the CPU time of the presented meshless formulation with the MLPG1 formulation and ANSYS. It should be noted that in the presented method, the domain integration over the sub-domains is eliminated and therefore, all numerical integrations were carried out only over the boundary of the sub-domains. Therefore, for the presented meshless method, the Gauss points in the radial direction i.e. n_r are eliminated and only the number of Gauss points in the circumferential direction, i.e. n_θ is reported in Table 2. As said before, circular sub-domain around the nodes is used in this study and the Gauss points are located on the boundary of the circles. It can be seen that elimination of the domain integration in the presented method yields to substantial reduction of the computational time. In all of the presented results 10 Gauss points are used for numerical integration on the boundary of the

Table 2: Comparison of the CPU time of the current meshless method and the MLPG1 method.

Method	Gauss point		Number of nodes	CPU Time (Sec)	E_1 (GPa)
	n_θ	n_r			
MLPG1 (Atluri and Zhu (2000))	5	5	528	35.2	147.93
Present method	5	–	528	10.4	147.15
MLPG1 (Atluri and Zhu (2000))	10	10	528	110.25	146.86
Present method	10	–	528	18.5	146.59
FEM (ANSYS)	–	–	1200	~26	146.19

sub-domains. The prediction of the finite element for effective transverse modulus is also included in Table 2. The prediction of present model for effective elastic modulus of the composite is between the predictions of the MLPG and ANSYS. The node distribution (computational model) which is used in the analysis of the RVE is shown in Fig. 3. In the analysis of the problem, a fourth-order spline-type function is used as the weight function in construction of the shape function via the MLS method. According to the node distribution in Fig. 3, the radius of support domain in construction of the shape function for nodes depend on the density of nodes located around that node. The radius of support domain is selected large enough so that at least a node in radial direction and a node in circumferential direction in the neighborhood of the node are located inside the support domain of that node or at least 4 neighborhood nodes locate in it. In general $r_{supp} = ad_{min}$ and $r_{test} = bd_{min}$ in which d_{min} is the distance between the node and nearest neighborhood node. a and b are chosen by the user. The choice of a is governed by the nodal arrangement, the dimension of the problem and the order of the monomial basis, whereas the choice of b depends only on the nodal arrangement. The test radius must be large enough so that the domain completely is covered. In this study a and b is chosen depends on the nodal distribution between 1.8 to 2.5. a usually is chosen about 2.5 and b is chosen about 1.8.

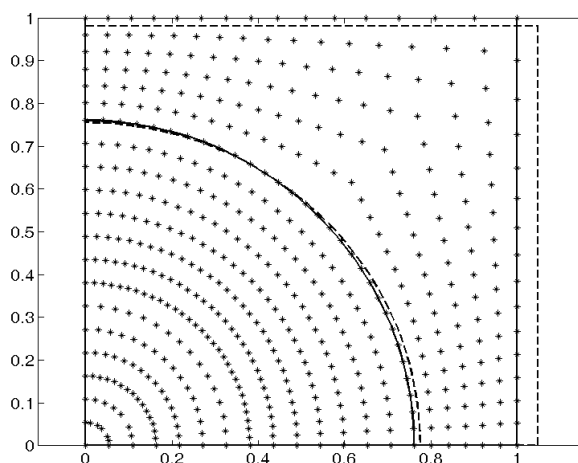


Figure 3: The nodal distribution form which is used in the meshless method, un-deformed (solid line), deformed scaled by 30 (dashed line).

Fig.3 shows the un-deformed and also the deformed shape of the RVE which is subjected to $\sigma_1^* = 180\text{MPa}$. The deformation of the RVE is exaggerated by a scale factor as 30.

6.2 Stress-strain response of B/Al composite

The stress-strain response of the B/Al composite in transverse loading is investigated in this section. The predicted elastic properties of the B/Al composite with 45.5% FVF are shown in Table 3. Also this table contains the predicted yield strength of the B/Al composite in the axial and transverse direction. As seen in Table 3, the predicted values of the present method are in excellent agreement with the predictions of the finite element analysis with ANSYS.

Table 3: The predicted elastic properties of Boron/Aluminum composite with 45.5% FVF.

Material Property	$E_1 = E_2$ (GPa)	E_3 (GPa)	ν_{12}	ν_{13}	ν_{31}	σ_{Y1} (MPa)	σ_{Y3} (MPa)
Meshless	146.591	219.618	0.2955	0.1758	0.2637	125.486	436.923
ANSYS	146.198	219.780	0.3099	0.1754	0.2637	124.56	436.921

The predicted elastic-plastic stress-strain response diagram of the B/Al composite with 45.5% fiber volume fraction in transverse loading is shown in Fig. 4. In this Figure, the overall stress level in each load step is plotted vs. the overall strain in the same step. The predictions of the presented meshless method and the finite element analysis with ANSYS are included in this Figure. As seen in Fig. 4, the predictions of the meshless and finite element method are in excellent agreement. The initial local yield stress of the composite in the transverse loading is predicted as $\sigma_{Y1} = 125.486$ MPa. It is seen that the presented meshless model shows excellent

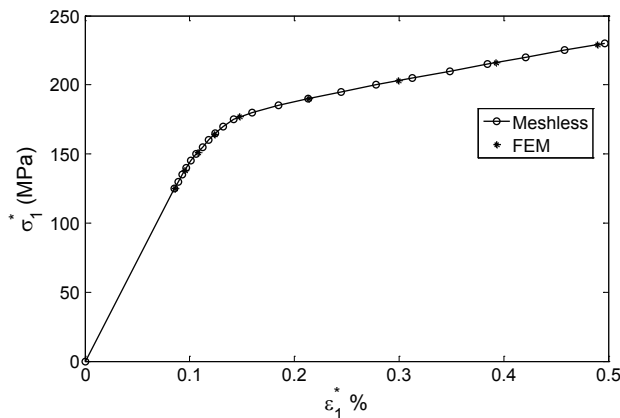


Figure 4: Stress-strain curve of B/Al metal matrix composite in transverse loading (45.5% FVF).

agreement with the finite element method in the prediction of the overall properties of the B/Al composite.

6.3 Displacement and micro-stresses

The distributions of the local field variables in the RVE subjected to transverse normal load are studied in this section. The distribution of displacement in the x_1 direction, u_1 , on the bottom path ($x_2 = 0, 0 < x_1 < a$) and on the top path ($x_2 = a, 0 < x_1 < a$) of the RVE for transverse applied load $\sigma_1^* = 180$ MPa are shown in Fig. 5. As expected, the distribution of the displacement is continuous in the fiber-matrix interface. Excellent agreement is seen between the meshless and the finite element method in the prediction of the displacement field in the RVE. The distribution of the micro-stresses, σ_1 , σ_2 , σ_3 and σ_{eff} on the bottom path of the RVE is shown in Fig. 6. As seen, the transverse stress σ_1 is continuous at the fiber-matrix interface. The axial stress σ_3 is compressive in the fiber and is tensile in the matrix and is discontinuous at the fiber-matrix interface. The transverse stress σ_2 is discontinuous at the interface. The distribution of the effective Von Mises stress σ_{eff} is shown in this Figure. On the bottom path, the matrix has been entered into the plastic region. As seen in Fig. 6, because the hardening modulus of the matrix in the plastic region is very small ($E_T = 1.17$ GPa), the distribution of σ_{eff} stress in the matrix on the bottom path is almost uniform. The distribution of the micro-stresses σ_1 , σ_2 , σ_3 and σ_{eff} on the left path ($x_1 = 0$) of the RVE for applied stress $\sigma_1^* = 180$ MPa is shown in Fig. 7. This load causes the plastic deformation in the matrix. As seen, on the left path, σ_2 stress is compressive and continuous at the

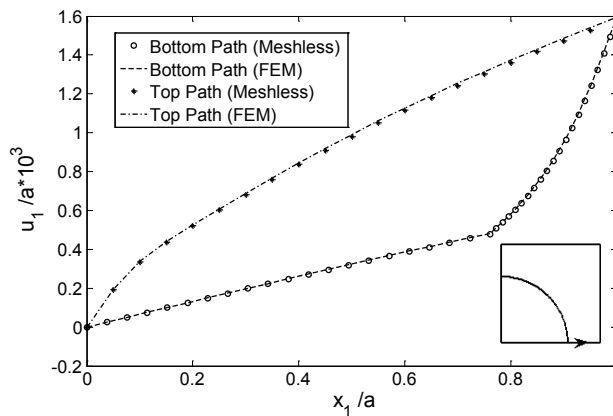


Figure 5: Distribution of displacement on the bottom and top path of the RVE ($\sigma_1^* = 180$ MPa).

fiber-matrix interface while the σ_1 , σ_2 and σ_{eff} are discontinuous at the interface. σ_1 and σ_{eff} in the fiber is larger than in the matrix.

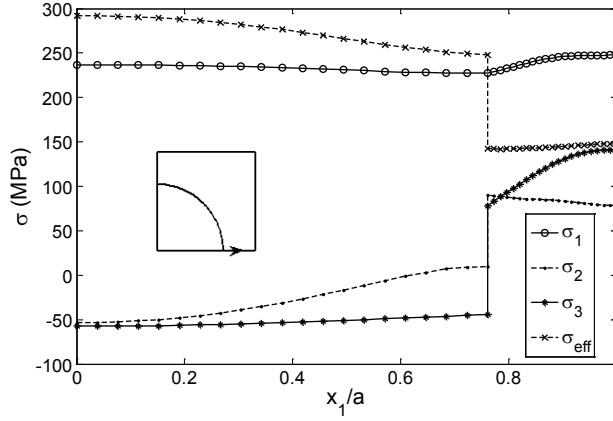


Figure 6: Distribution of micro-stresses σ_1 , σ_2 , σ_3 and σ_{eff} on the bottom path of the RVE, ($\sigma_1^* = 180\text{MPa}$).

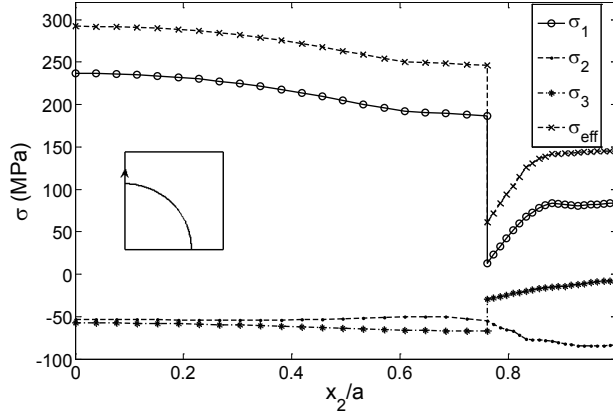


Figure 7: Distribution of micro-stresses σ_1 , σ_2 , σ_3 and σ_{eff} on the left path of the RVE, ($\sigma_1^* = 180\text{MPa}$).

6.4 Micro-strains

The distribution of the micro-plastic strains on the bottom path of the RVE for $\sigma_1^* = 180\text{ MPa}$ is shown in Fig. 8. As seen in Fig. 8, the ϵ_1^p is positive and ϵ_2^p and ϵ_3^p are negative on the bottom path. The equivalent plastic strain $\epsilon_{equ}^p \approx \epsilon_p$ is also shown

in this Figure. The maximum of ε_1^p which is occurred on the bottom path at point $(a, 0)$ is about 0.5%. In Fig. 8, for $x_1/a > 0.76$ plastic strains are observed in the matrix and for $x_1/a < 0.76$ the plastic strains are vanished. The distribution of micro-plastic strains on the left path of the RVE for $\sigma_1^* = 180\text{MPa}$ is shown in Fig. 9. As seen, for $x_2/a < 0.89$ the plastic strains are vanished. ε_1^p is positive and ε_2^p and ε_3^p is negative on this path.

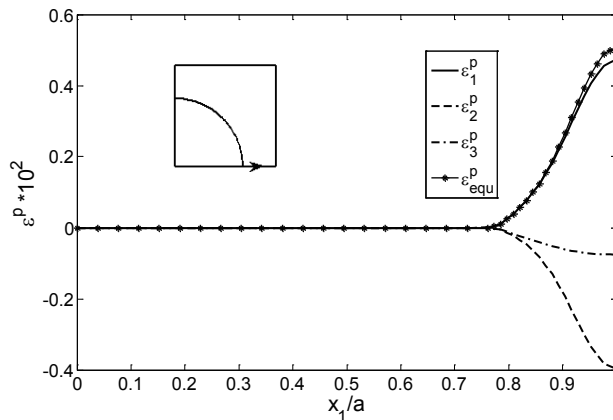


Figure 8: Distribution of micro-plastic strains ε_1^p , ε_2^p and ε_{equ}^p on the bottom path of the RVE, ($\sigma_1^* = 180\text{MPa}$).

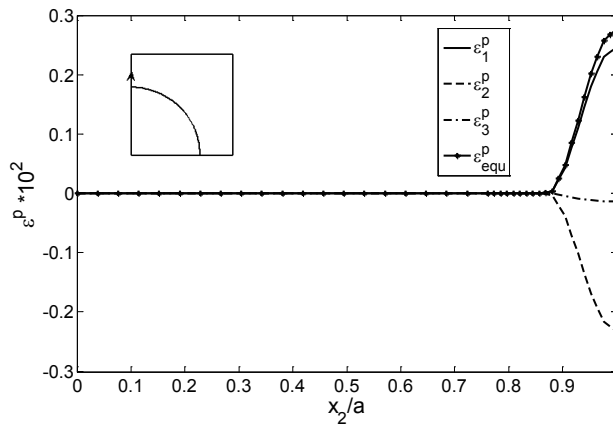


Figure 9: Distribution of micro-plastic strains ε_1^p , ε_2^p , ε_3^p and ε_{equ}^p on the left path of the RVE, ($\sigma_1^* = 180\text{MPa}$).

6.5 Elastic-plastic load reversal

In this section it is supposed that the RVE is loaded in the transverse direction to the macro-stress as $\sigma_1^* = 180$ MPa and then unloaded to 0 and reloaded to compressive transverse normal stress as $\sigma_1^* = -180$ MPa. The Prager’s linear kinematic hardening model is employed for the Aluminum. The distribution of the normal stresses on the bottom path of the RVE is shown in Fig. 10. This figure includes the normal stresses σ_1 , σ_2 , σ_3 and effective von misses stress σ_{eff} when the RVE is loaded in transverse x_1 direction from 0 to 180 MPa and the loaded to -180 Mpa. The σ_1 stress is compressive through the path and σ_2 is so that it integration on the path is vanished.

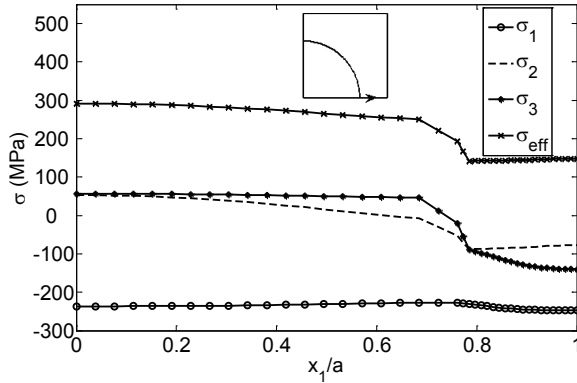


Figure 10: Distribution of micro-stresses σ_1 , σ_2 , σ_3 and σ_{eff} on the bottom path of the RVE, (loading to $\sigma_1^* = 180$ MPa and reloading to $\sigma_1^* = -180$ MPa).

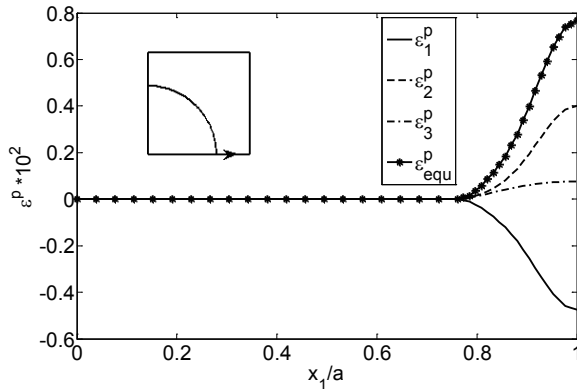


Figure 11: Distribution of micro-plastic strains ϵ_1^p , ϵ_2^p and ϵ_{equ}^p on the bottom path of the RVE, (loading to $\sigma_1^* = 180$ MPa and reloading to $\sigma_1^* = -180$ MPa).

The distribution of plastic strains ϵ_1^p , ϵ_2^p , ϵ_3^p and the equivalent plastic strain ϵ_{equ}^p on the bottom path of the RVE is shown in Fig. 11. As seen in the Fig.11, ϵ_1^p is negative on the path and ϵ_2^p and ϵ_3^p is positive. By comparison of Fig. 8 and Fig. 11, it is seen that the total plastic strain ϵ_{equ}^p in Fig. 11 is larger than ϵ_{equ}^p in Fig. 8.

7 Conclusions

In this study a meshless method based on the meshless local Petrov-Galerkin method is presented for the elastic-plastic analysis of solid structures. Because the domain integration is eliminated from the formulation, the computational cost is reduced. The well-known Prandtl-Reuss flow rule and the incremental theory of plasticity are used for the formulation of the nonlinearity of the problem due to the plastic strains. The presented method is formulated for the generalized plane strain case. The presented meshless method is conjugated with a generalized plane strain micromechanical model for the analysis of the elastic-plastic behavior of the unidirectional composite materials. The fully bonded interface is considered and a direct method is developed to enforce the continuity of displacement and traction at the fiber-matrix interface. The Euler integration method is employed for the integration of the discrete governing differential equations of the system. The Boron/Aluminum metal matrix composite subjected to transverse loading condition is studied. The predicted results for the overall and local response of Boron/Aluminum show good agreement with the predictions of the finite element method.

Appendix

To determine the unknown parameter $d\lambda$ in the Prandtl-Reuss flow rule, Eq. (6) is multiplied by itself and is written as

$$d\lambda = [d\epsilon_{ij}^p d\epsilon_{ij}^p]^{1/2} / (S_{ij} S_{ij})^{1/2} \quad (A1)$$

The effective stress σ_e , and the effective plastic strain increment $d\epsilon_p$ are defined as

$$\begin{aligned} \sigma_e &= \left(\frac{3}{2} S_{ij} S_{ij} \right)^{1/2} \\ d\epsilon_p &= \left(\frac{2}{3} d\epsilon_{ij}^p d\epsilon_{ij}^p \right)^{1/2} \end{aligned} \quad (A2)$$

Now, by employing (A2) in (A1), the parameter $d\lambda$ and the plastic strain increment can be obtained in terms of $d\epsilon_p$ and σ_e as

$$d\lambda = \frac{3}{2} \frac{d\epsilon_p}{\sigma_e} \quad (A3)$$

$$d\epsilon_{ij}^p = \frac{3}{2} \frac{d\epsilon_p}{\sigma_e} S_{ij} \quad (\text{A4})$$

In order to establish a relationship between the effective stress σ_e and the effective plastic strain increment $d\epsilon_p$, the uniaxial tensile test in the plastic region is considered. In the uniaxial tensile test, σ_e and $d\epsilon_p$ will be obtained as

$$\begin{aligned} \sigma_e &= \sigma_{11} \\ d\epsilon_p &= d\epsilon_{11}^p \end{aligned} \quad (\text{A5})$$

and the plastic strain increment in the uniaxial loading can be obtained as

$$d\epsilon_{11}^p = d\epsilon_{11} - d\epsilon_{11}^e = \left(\frac{1}{E_T} - \frac{1}{E} \right) d\sigma_{11} \quad (\text{A6})$$

In which $E_T = d\sigma/d\epsilon$ is the hardening modulus of the material in the plastic region and E is the elastic module of the material. By substituting Eq. (A5) in Eq. (A6) it can be concluded that

$$d\epsilon_p = \left(\frac{1}{E_T} - \frac{1}{E} \right) d\sigma_e = \frac{d\sigma_e}{M_T} \quad (\text{A7})$$

where

$$M_T = d\sigma_e/d\epsilon_p = \left(\frac{1}{E_T} - \frac{1}{E} \right)^{-1} \quad (\text{A8})$$

By substituting Eq. (A7) into Eq. (A3), the parameter $d\lambda$ can be obtained as

$$d\lambda = \frac{3}{2} \frac{d\epsilon_p}{\sigma_e} = \frac{3}{2} \frac{d\sigma_e}{\sigma_e M_T} \quad (\text{A9})$$

By differentiating Eq. (A2), $d\sigma_e$ may be obtained.

$$d\sigma_e = \frac{3S_{ij}}{2\sigma_e} dS_{ij} \quad (\text{A10})$$

and substitution of Eq. (A10) into Eq. (A9) yields

$$d\lambda = \frac{9}{4} \frac{S_{ij} dS_{ij}}{\sigma_e^2 M_T} \quad (\text{A11})$$

In the theory of plasticity, it is usually assumed that no plastic work can be done by the hydrostatic component of stress, i.e.

$$S_{ij} dS_{ij} = S_{ij} (d\sigma_{ij} - \frac{1}{3} d\sigma_{kk} \delta_{ij}) = S_{ij} d\sigma_{ij} \quad (\text{A12})$$

So, $d\lambda$ can be obtained by the substituting Eq. (A12) into Eq. (A11) as

$$d\lambda = \frac{9 S_{ij} d\sigma_{ij}}{4 \sigma_e^2 M_T} \quad (\text{A13})$$

The total strain increment $d\epsilon_{ij}$ can be calculated by substituting Eq. (6) in the strain-stress relation in Eq. (4) as

$$d\epsilon_{ij} = \frac{1}{2G} d\sigma_{ij} - \frac{\nu}{E} d\sigma_{kk} \delta_{ij} + d\lambda S_{ij} \quad (\text{A14})$$

The sides of this equation are multiplied by S_{ij} as

$$S_{ij} d\epsilon_{ij} = \frac{1}{2G} S_{ij} d\sigma_{ij} - \frac{\nu}{E} d\sigma_{kk} \delta_{ij} S_{ij} + d\lambda S_{ij} S_{ij} \quad (\text{A15})$$

The first term in the right side of Eq. (A15) can be rewritten using Eq. (A13) as

$$\frac{1}{2G} S_{ij} d\sigma_{ij} = \frac{2}{9G} \sigma_e^2 M_T d\lambda \quad (\text{A16})$$

and the second term in the right side of Eq. (A15) can be written as

$$\frac{\nu}{E} d\sigma_{kk} \delta_{ij} S_{ij} = \frac{\nu}{E} d\sigma_{kk} S_{ii} = 0 \quad (\text{A17})$$

By employing Eq. (A16), (A17) and (A2), Eq. (A15) can be rewritten as

$$S_{ij} d\epsilon_{ij} = \frac{2}{9G} \sigma_e^2 M_T d\lambda + \frac{2}{3} d\lambda \sigma_e^2 \quad (\text{A18})$$

Now, $d\lambda$ can be obtained in terms of $d\epsilon_{ij}$ as

$$d\lambda = \frac{S_{ij} d\epsilon_{ij}}{\frac{2}{3} \sigma_e^2 (1 + \frac{1}{3G} M_T)} \quad (\text{A19})$$

References

Aboudi, J. (1996): Micromechanical analysis of composites by the method of cells-update. *Appl. Mech. Rev.*, vol. 49, no. 10, pp. S83–S91.

Adams, D. F. (1970): Inelastic analysis of unidirectional composite subjected to transverse normal loading. *J. Comp. Mater.*, vol. 4, pp. 310–328.

Adams, D. F.; Crane, D. A. (1984): Combined loading micromechanical analysis of a unidirectional composite. *Composites*, vol. 15, no. 3, pp. 181–192.

Aghdam, M. M.; Smith, D. J.; Pavier, M. J. (2000): Finite element micromechanical modelling of yield and collapse behaviour of metal matrix Composites. *J. Mech. Phys. Solids*, vol. 48, pp. 499–528.

Ahmadi, Isa; Aghdam, M. M. (2010): A generalized plane strain meshless local Petrov-Galerkin method for the micromechanics of thermo-mechanical loading of composites, *Journal of Mechanics of Materials and Structures*, vol. 5, no. 4, pp. 549–566.

Ahmadi, Isa; Aghdam, M. M. (2011a): Heat transfer in composite materials using a new truly local meshless method. *International Journal of Numerical Methods for Heat & Fluid Flow*, vol. 21, no. 3, pp. 293–309.

Ahmadi, Isa; Aghdam, M. M. (2011b): A truly generalized plane strain meshless method for combined normal and shear loading of fibrous composites. *Engineering Analysis with Boundary Elements*, vol. 35, pp. 395–403.

Arnoled, S. M.; Pindera, M. J.; Wilt, T. E. (1996): Influence of fiber architecture on the inelastic response of metal matrix composites. *Int. J. of Plasticity*, vol. 12, pp. 507–545.

Atluri, S. N.; Shen, S. (2002): The meshless local Petrov-Galerkin (MLPG) method: a simple & less-costly alternative to the finite element and boundary element methods. *CMES: Computer Modeling in Engineering & Sciences*, vol. 3, no. 1, pp. 11–51.

Atluri, S. N. (2004): The meshless method (MLPG) for domain and BIE discretizations, Tech Science Press, Forsyth.

Atluri, S. N.; Zhu, T. (1998): A new meshless local Petrov-Galerkin (MLPG) approach in computational mechanics. *Comput. Mech.*, vol. 22, pp. 117–127.

Atluri, S. N.; Zhu, T. (2000): The meshless local Petrov-Galerkin (MLPG) approach for solving problems in elastostatics. *Comput. Mech.*, vol. 25, pp. 169–179.

Batra, R. C.; Porfiri, M. (2008): Analysis of rubber-like materials using meshless local Petrov-Galerkin (MLPG) method. *Commun. Numer. Meth. En.*, vol. 24, no. 12, Sp. Iss. SI, pp. 1781–1804.

Belinha, J.; Dinis, L. M. J. S. (2006): Analysis of plates and laminates using the element-free Galerkin method. *Comput. Struct.*, vol. 84, pp. 1547–1559.

Belytschko, T.; Lu, Y. Y.; Gu, L. (1995): Crack propagation by element free galerkin methods. *Eng. Frac. Mech.*, vol. 51, no. 2, pp. 211–222.

Belytschko, T.; Lu, Y. Y.; Gu, L. (1994): Element-free Galerkin methods. *Int. J. Numer. Methods Engrg.*, vol. 37, pp. 229–256.

Ching, H. K.; Batra, R. C. (2001): Determination of crack tip fields in linear elastostatics by the meshless local Petrov-Galerkin (MLPG) method. *CMES: Computer Modeling in Engineering & Sciences*, vol. 2, no. 2, 273–290.

Coker, D.; Ashbaugh, N. E.; Nicholas, T. (1993): Analysis of thermomechanical cyclic behavior of unidirectional metal matrix composites. *Thermomechanical fatigue Behavior of Materials, ASTM STP* vol. 1186, Sehitoglu ed. pp. 50–69.

Dai, K. Y.; Liu, G. R.; Han, X.; Li, Y. (2006): Inelastic analysis of 2D solids using a weak-form RPIM based on deformation theory. *Comput. Methods Appl. Mech. Engrg.*, vol. 195, pp. 4179–4193.

Ding, S. R.; Tong, J. W.; Shen, M. (2005): Numerical simulation of elastic-plastic behavior of thermoplastic composites. *J. Reinf. Plast. Comp.*, vol. 24, pp. 649–655.

Dong, L.; Alotaibi, A.; Mohiuddine, S. A.; Atluri, S. N. (2014): Computational methods in engineering: a variety of primal & mixed methods, with global & local interpolations, for well-posed or Ill-Posed BCs, *CMES: Computer Modeling in Engineering & Sciences*, vol. 99, no. 1, pp.1–85.

Duarte, C. A. M.; Oden, J. T. (1996): An h-p adaptive method using clouds. *Comput. Methods Appl. Mech. Engrg.*, vol. 139, pp. 237–262.

Dvorak, G. J.; Bahei-El-Din, Y. A. (1979): Elastic-Plastic behaviour of fibrous composite. *J. Mech. Phys. Solids*, vol. 27, pp. 51–72.

Dvorak, G. J.; Bahei-El-Din, Y. A. (1982): Plasticity Analysis of fibrous composite. *ASME J. Appl. Mech.*, vol. 49, pp. 327–335.

Foye, R. L. (1973): Theoretical post-yielding of behaviour of composite laminates, Part I- Inelastic micromechanics. *J. Comp. Mater.*, vol. 7, pp. 178–193.

Gu, Y. T.; Liu, G. R. (2001): A meshless local Petrov-Galerkin (MLPG) formulation for static and free vibration analysis of thin plates. *CMES: Computer Modeling in Engineering & Sciences*, vol.2, no. 4, pp. 463–476.

Gu, Y. T.; Liu, G. R. (2002): A boundary point interpolation method for stress analysis of solids. *Comput. Mech.*, vol. 28, 47–54.

Gu, Y. T.; Wang, Q. X.; Lam, K. Y.; Dai, K. Y. (2007): A pseudo-elastic local meshless method for analysis of material nonlinear problems in solids. *Eng. Anal. Bound. Elem.*, vol. 31, pp. 771–782.

Han, Z. D.; Rajendran, A. M.; Atluri, S. N. (2005): Meshless local Petrov-Galerkin (MLPG) approaches for solving nonlinear problems with large deformations and rotations, *CMES: Computer Modeling in Engineering & Sciences*, vol. 10, no. 1, pp. 1–12.

Heaney, C.; Augarde, Ch.; Deeks, A. (2010): Modelling Elasto-Plasticity Using the Hybrid MLPG Method. *CMES: Computer Modeling in Engineering & Sciences*, vol. 56, no. 2, pp. 153–177.

Hill, R. (1964): Theory of mechanical properties of fiber-strengthened materials. II. Inelastic Behaviour. *J. Mech. Phys. Solids*, vol. 12, pp. 213–218.

Hill, R. (1965): Theory of mechanical properties of fiber-strengthened materials. III. Self-Consistent Model, *J. Mech. Phys. Solids*, vol. 13, pp. 189–198.

Huang, Z. M. (2000): A unified micromechanical model for the mechanical properties of two constituent composite materials Part II: Plastic behavior. *J. Thermo-plastic Comp. Mater.*, vol. 13, pp. 344–362.

Hung, W. (1973): Elastoplastic transverse properties a unidirectional fiber reinforced composites. *J. Comp. Mater.*, vol. 7, pp. 482–499.

Li, G.; Belytschko, T. (2001): Element-free Galerkin method for contact problems in metal forming analysis. *Eng. Comput.*, vol. 18, pp. 62–78.

Lin, H.; Atluri, S. N. (2001): The meshless local Petrov-Galerkin (MLPG) method for solving incompressible Navier-Stokes equations. *CMES: Computer Modeling in Engineering & Sciences*, vol. 2, pp. 117–142.

Lin, T. H.; Salinas, D.; Ito, Y. M. (1972): Initial yeild surface of a unidirectionally reinforced composite. *ASME J. Appl. Mech.*, vol. 39, pp. 321–329.

Liu, W. K.; Chen, Y.; Chang, C. T.; Belytschko, T. (1996): Advances in multiple scale kernel particle methods. *Comput. Mech.*, vol. 18, pp. 73–111.

Long, S. Y.; Liu, K. Y.; Hu, D. A. (2006): A new meshless method based on MLPG for elastic dynamic problems. *Eng. Anal. Bound. Elem.*, vol. 30, 43–48.

Mendelson, A. (1970): *Plasticity: Theory and Application*. MacMillan, New York.

Mukherjee, Y. X.; Mukherjee, S. (1997): Boundary node method for potential problems. *Int. J. Numer. Methods Engrg.*, vol. 40, pp. 797–815.

Nayroles, B.; Touzot, B.; Villon, P. (1992): Generalizing the finite element method: diffuse approximation and diffuse elements. *Comput. Mech.*, vol. 10, pp. 307–318.

Perez Pozo, L.; Perazzo, F.; Angulo, A. (2009): A meshless FPM model for solving nonlinear material problems with proportional loading based on deformation theory. *Adv. Eng. Software*, vol. 40, pp. 1148–1154.

Robertson, D. D.; Mall, S. (1993): Micromechanical relation for fiber reinforced composites using a free transverse shear approach. *J. Comp. Tech. and Res.*, vol. 15, pp. 181–192.

Singh, I. V.; Sandeep, K.; Prakash, R. (2002): The element free Galerkin method in three-dimensional steady state heat conduction. *Int. J. Comput. Eng. Sci.*, vol. 3, pp. 291–303.

Sladek, J.; Sladek, V.; Tan, C. L.; Atluri, S. N. (2008): Analysis of transient heat conduction in 3D anisotropic functionally graded solids by the MLPG, *CMES: Computer Modeling in Engineering & Sciences*, vol. 32, pp. 161–174.

Sladek, J.; Sladek, V.; Atluri, S. N. (2004): Meshless local Petrov-Galerkin method for heat conduction problem in an anisotropic medium. *CMES: Computer Modeling in Engineering & Sciences*, vol. 6, no. 3, pp. 309–318.

Sladek, J.; Sladek, V.; Solek, P. (2009): Elastic analysis in 3D anisotropic functionally graded solids by the MLPG, *CMES: Computer Modeling in Engineering & Sciences*, vol. 43, no. 3, pp. 223–251.

Sladek, J.; Stanak, P.; Han, Z-D.; Sladek, V.; Atluri, S. N. (2013): Applications of the MLPG method in engineering & sciences: A review, *CMES: Computer Modeling in Engineering & Sciences*, vol. 92, no. 5, pp. 423–475.

Sukumar, N.; Moran, B.; Belytschko, T. (1998): The natural element method. *Int. J. Numer. Methods Engrg.*, vol. 43, pp. 829–887.

Sun, C. T.; Chen, J. L. (1991): A Micromechanical Model for Plastic Behavior of Fibrous Composites. *Comp. Sci. Tech.*, vol. 40, pp. 115–129.

Taliencio, A. (2005): Generalized plane strain finite element model for the analysis of elastoplastic composites. *Int. J. Solids Struct.*, vol. 42, pp. 2361–2379.

Zhu, C.; Sun, C. T. (2003): Micromechanical Modeling of Fiber Composites Under Off-Axis Loading. *J. Thermoplastic Comp. Mater.*, vol. 16, pp. 333–344.

Zhu, T.; Zhang, J.-D.; Atluri, S. N. (1998): A local boundary integral equation (L-BIE) method in computational mechanics, and a meshless discretization approach. *Comput. Mech.*, vol. 21, pp. 223–235.